ELSEVIER

# Orientation and partitioning behavior of dilute rodlike polyelectrolyte suspensions within confined slit microchannels

Myung-Suk Chun [a],*, Sang Il Kim [a], O  Ok Park [b]

[a] *Complex Fluids and Membrane Laboratory*, *Korea Institute of Science and Technology*, *PO Box 131*, *Cheongryang*, *Seoul 130-650*, *South Korea*
[b] *Department of Chemical Engineering*, *Korea Advanced Institute of Science and Technology*, *Kusong-dong*, *Yusung-ku*, *Taejon 305-701*, *South Korea*

## Abstract

In the confined space of narrow channels, the behavior of rodlike polyelectrolytes pertaining to anisotropic configuration effect is much different than in the bulk. Based on our previous study, we analyzed on the orientational order of rodlike polyelectrolyte in dilute suspensions under the action of the long-range colloidal interactions, which results in the concentration depletion near the solid surface. For the orientation of rodlike polyelectrolytes existing near the charged wall, the electrostatic repulsive interaction explicitly creates the preferential alignment of rod segments perpendicular to the surface, while the parallel alignment is favored without this interaction. The concentration-depleted layer thickness, in which the perpendicular orientation of the rods is predicted, increases either with decreased solution ionic strength or with increased surface potentials of the wall and the rod. The partition coefficient determined from the concentration profile presents the fact that the rod is more excluded by electrostatic and entropic effects with the increase of confining strength. It is evident that the presence of electrostatic interactions changes the partitioning behavior of rodlike polyelectrolyte suspension in the dilute limit. © 2002 Elsevier Science B.V. All rights reserved.

*Keywords:* Confined spaces; Long-range interaction; Orientational order; Concentration partitioning; Rodlike polyelectrolytes

## Nomenclature

$A_H$    Hamaker constant
$a$      $(R_p^2 + \lambda^2)^{1/2}$

---

\* Corresponding author. Fax: + 82-2-958-5308.
*E-mail address:* mschun@kist.re.kr (M.-S. Chun).

| | |
|---|---|
| $b$ | $[R_p^2 + (L - \lambda)^2]^{1/2}$ |
| $C$ | segment density |
| $C_m$ | monomer density |
| $d$ | apparent depleted layer thickness |
| $e$ | elementary electric charge |
| $f$ | orientational order parameter |
| $K$ | partition coefficient |
| $kT$ | Boltzmann thermal energy |
| $L$ | length of rodlike polyelectrolyte |
| $\boldsymbol{n}$ | unit vector |
| $n_1$ | line density of atoms along the axis of symmetry of the rod |
| $P$ | penetration depth |
| $R_p$ | radius of polyelectrolyte |
| $s$ | scalar parameter specifying a position along the row of atoms |
| $\boldsymbol{u}$ | anisotropic-particle direction vector |
| $\boldsymbol{x}$ | coordinate vector describing particle position |
| $x$ | distance from the wall to $\lambda$ point of rod |
| $x'$ | distance excluding the closest approach distance from x |
| $x_c$ | distance from the wall to the local row-position variable s |
| $x_s$ | x coordinate of random position located at a radial surface of rod |
| $y$ | $\cos \theta$ |
| $z$ | valence |

*Greek letters*

| | |
|---|---|
| $\kappa$ | inverse Debye length |
| $\lambda$ | arbitrary point on the rod fixed to position $x$ |
| $\boldsymbol{\xi}$ | coordinate vector describing particle orientation |
| $\rho$ | azimuthal angle around the rod cross section |
| $\sigma$ | dimensionless surface charge density |
| $\Phi$ | interaction energy between wall and polyelectrolyte |
| $\psi$ | dimensionless electrostatic potential |
| $\psi_s$ | dimensionless electrostatic surface potential |
| $\Omega$ | time-averaged probability of finding a rod |
| $\Omega_0$ | probability density function in bulk solution |

*Subscripts*

| | |
|---|---|
| DL | electrostatic double layer repulsion |
| p | polyelectrolyte |
| VW | van der Waals attraction |
| w | wall |

*Superscripts*

| | |
|---|---|
| * | dimensionless |

## 1. Introduction

The polyelectrolyte, that is a kind of complex fluid, is a polymer chain carrying ionizable groups. While the behavior of uncharged polymer solutions is well understood, polyelectrolyte solutions still present experimental and theoretical challenge [1]. In confined spaces, the behavior of anisotropic rodlike polyelectrolytes associated with configuration effects can be much different from that in bulk solutions, in which the concentration depletion is observed near a wall surface. The concentration depletion results in both the apparent slip effects and the velocity enhancement of the rodlike polyelectrolytes relative to the solvent molecules.

Several simple models have been proposed to describe rigid polyelectrolyte behavior near boundaries when the contacting suspension is dilute and adsorption can be neglected. Note that Auvray [2] considered the depleted layer for rodlike polymers in a narrow capillary or near a large spherical particle. He obtained closed form analytical solutions which have been used by previous researchers [3,4]. The existence of depleted layers in polyelectrolyte solutions of anionic xanthan subject to simple shear flow has been observed by using evanescent wave-induced fluorescence techniques [5,6]. Regarding the rigid rodlike polyelectrolytes in a narrow capillary, Sorbie [7] extended the two-fluid approach by considering the effects of the concentration-depleted layer on rheological and transport properties. Later, de Pablo et al. [8] have demonstrated the changes of depleted layer under simple shear flow by employing stochastic computations on the dilute suspension of uncharged rodlike polymers.

In the early 1990s, Chun et al. [9] presented the analysis on the development of concentration-depleted layer and the corresponding experimental results for semiflexible polyelectrolytes using capillary hydrodynamic fractionation system. Extending the previous formalism [10] for the problem of infinitesimally thin rod–wall interaction, they developed a theoretical model predicting the chain configuration of rodlike polyelectrolytes relative to the confining wall boundary. The surface charge model of the rod ensures a more rigorous

analysis for more realistic system of polyelectrolytes compared with that of the line charge density. Their results showed that the concentration profiles shift markedly toward the center of the capillary either with decreased ionic strength of the eluant suspension or with increased surface potentials of a wall and the polyelectrolyte.

The axisymmetric rodlike conformation is a one of the simple non-spherical shapes and it results in the rod orientation, which can be an important microstructural property of polyelectrolyte suspension. The orientational order parameter represents how perfectly the rodlike polyelectrolytes are oriented along unit vector. As an another significant property of rodlike polyelectrolytes, we need to examine the concentration partitioning behavior. In principle, the partition coefficient is a reflection of the probability of finding the particle within the bulk-like region of the confined channel, averaged over the channel cross section. Many studies on the partitioning of charged spherical colloids have been performed in the limit of infinite dilution [11,12] as well as at moderate particle concentrations [13,14]. For the partitioning problem of non-spherical colloids such as a rodlike polyelectrolyte, several studies have been reported for the purely steric case in the limit of infinite dilution [3,15]. When the long-range interactions are involved, however, it is hard to find the published results even in the limit of infinite dilution.

It is necessary to point out that the evaluation of long-range interaction energies in respect to random orientations should be solved unambiguously so as to conduct the rodlike polyelectrolyte. The starting point for understanding the complex behavior of rodlike polyelectrolytes is to consider a single rod in a dilute suspension, where the rod particles do not interact. As a further and continued work of the previous study, both the orientation and the concentration partitioning behavior of rodlike polyelectrolytes are theoretically investigated in the present paper. The calculated results stimulate the experimental study and suggest how these properties are closely related to the physicochemical phenomena of concentration depletion in confined spaces of slit microchannel.

## 2. Basic consideration on rod-wall physicochemical interaction

### 2.1. Rod configuration

Two-surface geometry of a slit microchannel is considered here like as in our previous study [9], we hence do not rewrite in detail. From the configurational statistics of polyelectrolyte chain, the configuration partition function of a rod depends explicitly on its orientation. The time-averaged probability $\Omega$ of finding a rod with orientation $\xi$ at any position is given by the Boltzmann expression. The segment density $C$ is obtained by integrating $\Omega$ over all of the orientation angular space:

$$C = \int_{\text{Domain}} \Omega d\xi = \int_{\text{Domain}} \Omega_0 \exp\left[\frac{-\Delta\Phi}{kT}\right] d\xi \quad (1)$$

where $\Phi$ is the interaction energy pertaining to long-range colloidal forces between the rod and the nearby wall, $kT$ the Boltzmann thermal energy, and $\Omega_0$ the probability density function in the bulk.

Since the segment density $C$ in Eq. (1) corresponds to the center-of-mass number density of rods, we need to deal with a monomer density that is the most accessible to experimental verifications [10]. In Fig. 1, the segment density profile $C(\lambda, x)$ was defined as a function of an arbitrary point $\lambda$ on the rod with length $L$ fixed to position $x$, where $L/2 < \lambda < L$. Then, the monomer density $C_m(x)$ can be obtained by integrating $C(\lambda, x)$ at $x$ over all the segment density. The rod length $L$ is taken less than the half width of channel, and we consider the thin rod in the present study so that the length $L$ is much larger than the rod radius $R_p$. The monomer density is derived as follows:

$$C_m(x) = \frac{\int_{L/2}^{L} C(\lambda, x)d\lambda}{\int_{L/2}^{L} d\lambda} = \begin{cases} \frac{2}{L}\left(\int_{L/2}^{L-x} C^{\text{I}}(\lambda, x)d\lambda + \int_{L-x}^{L} C^{\text{II}}(\lambda, x)d\lambda\right) & x' < \frac{L}{2} \\ \frac{2}{L}\left(\int_{L/2}^{x} C^{\text{I}}(\lambda, x)d\lambda + \int_{x}^{L} C^{\text{II}}(\lambda, x)d\lambda\right) & \frac{L}{2} < x' < L \\ \frac{2}{L}\int_{L/2}^{L-x} C^{\text{III}}(\lambda, x)d\lambda & x' > L. \end{cases} \quad (2)$$
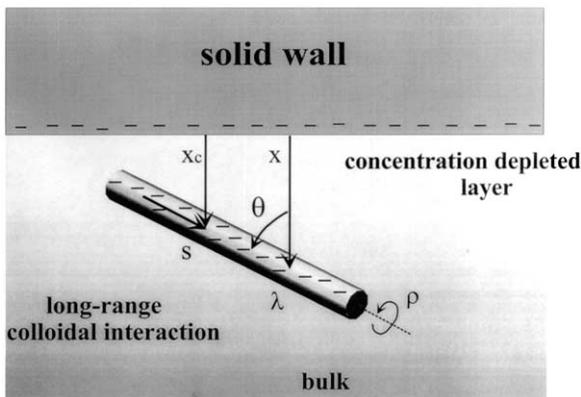


Fig. 1. Schematic representation of a negatively-charged rod in the vicinity of a like-charged wall with the variables employed to define the configuration of polyelectrolyte relative to a neighboring surface. Due to the concentration depletion, the color becomes lighter with approach to the wall.

Here, $C(\lambda, x)$ is determined from the fact that the number of configurations for each $(\lambda, x)$ pair is proportional to the domain area of the spherical envelope defined by rotation of the longer end of a given rod about the position $x$. As provided in Table 1, three cases can be defined according to the rod position. The closest approach distance taken as 5 nm is introduced as done previously to treat the short-range solvation force in aqueous media.

### 2.2. Long-range colloidal interactions

Detailed descriptions regarding the interaction energies have also been provided in the previous paper [9]. The attractive van der Waals dispersion forces between two atoms or small molecules are additive and act over a relatively long range. The net interaction energy of a molecule and the pla-

Table 1
Classification of the segment density for rod configurations

| Contact with the confining wall | Segment density | Configurations |
|---|---|---|
| Contact by either the longer or shorter end of the rod $(R_p < x' < b)$ | $C^I(\lambda, x)$ | $\frac{1}{2}\int_{-x'/b}^{x'/a}\exp(-\Delta\Phi/kT)$ $d\cos\theta$ |
| Contact by the longer end $(b < x' < a)$ | $C^{II}(\lambda, x)$ | $\frac{1}{2}\int_{-1}^{x'/a}\exp(-\Delta\Phi/kT)$ $d\cos\theta$ |
| No possible contact $(x' > a)$ | $C^{III}(\lambda, x)$ | $\frac{1}{2}\int_{-1}^{1}\exp(-\Delta\Phi/kT)$ $d\cos\theta$ |

a, distance between $\lambda$ and the longer end of the rod, it equals to $(R_p^2 + \lambda^2)^{1/2}$; b, distance between $\lambda$ and the shorter end of the rod, it equals to $[R_p^2 + (L - \lambda)^2]^{1/2}$; $x'$, distance excluding the closest approach distance from $x$.

nar solid body of like molecules can be determined by a pairwise summation [16]. Considering the rod configuration with its cross-sectional area and applying the Dirac delta function, the attractive interaction potential is then obtained by:

$$\Phi_{vw} = n_l \int_0^L \Phi_{VW}(x_c)ds = -\frac{A_H R_p^2}{6}\int_0^L \frac{ds}{x_c^3}. \tag{3}$$

Here, $n_l$ denotes the line density of atoms along the axis of symmetry of the rod, $A_H$ the Hamaker constant, $x_c$ $(= x - \cos\theta(\lambda - s))$ the distance from the wall corresponding to the local position variable $s$ on the axis, and $s$ $(0 < s < L)$ the parameter specifying a position along the row of atoms.

We assume here that the rod has a uniform surface charge distribution. In principle, the linear superposition of the potentials around the separate bodies yields an electrostatic energy correct asymptotically in the large separation limit. By applying the Dirac delta function again, the electrostatic interaction energy is rewritten as the integral of the surface charge density of rod $\sigma_p$ multiplied by the potential exerted by the wall $\psi_w$ at each point occupied by the surface charge. With $\psi_w(x_s)$ made dimensionless by $ze/kT$ for $z$–$z$

type electrolyte, one can find the following equation:

$$\Phi_{DL} = \sigma_p R_p \int_0^{2\pi}\int_0^L \frac{kT}{ze}\psi_w(x_s)ds\,d\rho \tag{4}$$

where $e$ is the elementary electric charge, $\rho$ the azimuthal angle around a rod cross section, and $x_s$ the $x$ coordinate of an arbitrary position located at the rod surface (i.e. $x_s = x_c - R_p(1 - \cos^2\theta)^{1/2}\cos\rho$). It is noteworthy that, in Eq. (4), the presence of the thin rod can be ignored. Considering the finite diameter of the rod in the present study can favorably overcome the limit condition with the Debye–Hückel approximation. The electrostatic potential $\psi_w$ in an aqueous solution induced by the charge on the wall is determined by the full Poisson–Boltzmann equation [16,17]:

$$\nabla^2\psi_w - \kappa^2\sinh\psi_w = 0 \tag{5}$$

where $\kappa$ means the inverse Debye length taking $\kappa$ (nm$^{-1}$) = $3.278 \times$ [solution ionic strength (Mol)]$^{1/2}$ for aqueous condition.

In most cases of aqueous system, constant charge boundary conditions are more satisfactory, which take the form:

$$\boldsymbol{n}\cdot\nabla\psi_w = \sigma_w \quad \text{at } x_s = 0 \tag{6a}$$

$$\psi_w \text{ and } \boldsymbol{n}\cdot\nabla\psi_w \to 0 \quad \text{as } x_s \to \infty. \tag{6b}$$

Here, $\sigma_w$ is the dimensionless surface charge density of the wall alternatively expressed in terms of the surface potential of the wall $\psi_w$. It is well known that the potential field near a flat wall can yield an exact solution of Eq. (5), expressed as:

$$\psi_w(x_s) = 2\ln\left[\frac{1 + \tanh(\psi_{s,w}/4)\exp(-\kappa x_s)}{1 - \tanh(\psi_{s,w}/4)\exp(-\kappa x_s)}\right]. \tag{7}$$

The relationship between surface charge density and surface potential for a non-interacting rod can be derived by means of the perturbation method to the Poisson–Boltzmann equation in cylindrical coordinates. Under the assumption of uniform charge distribution, we obtained more rigorous solution for the dimensionless surface charge density of a rod $\sigma_p$ in powers of $(\kappa R_p)^{-1}$ up to $O[(\kappa R_p)^{-2}]$. It is expressed as:

$$\sigma_{\mathrm{p}} = \sinh\left(\frac{\psi_{\mathrm{s,p}}}{2}\right)$$

$$\times \sqrt{1 + \frac{1}{\cosh^2(\psi_{\mathrm{s,p}}/4)}\left(\frac{1}{\kappa R_{\mathrm{p}}}\right) + \frac{2\ln[\cosh(\psi_{\mathrm{s,p}}/4)]}{\sinh^2(\psi_{\mathrm{s,p}}/2)}\left(\frac{1}{\kappa R_{\mathrm{p}}}\right)^2}$$

(8)

where $\psi_{\mathrm{s,p}}$ is the potential on the isolated rod as the separation grows very large. As the rod approaches the wall, the surface potentials change due to the rod-wall interactions. However, the present model has been guaranteed in the asymptotic sense, because the attractive van der Waals force increases much faster and clearly dominates over the electrostatic force as the rod approaches closely the wall. From Eqs. (3) and (4), the Boltzmann factor can be obtained as follows:

$$\exp\left(-\frac{\Delta\Phi}{kT}\right)$$
$$= \exp\left[\frac{A_{\mathrm{H}} R_{\mathrm{p}}^2}{6}\int_0^L \frac{\mathrm{d}s}{x_{\mathrm{c}}^3} - \frac{\sigma_{\mathrm{p}} R_{\mathrm{p}}}{ze}\int_0^{2\pi}\int_0^L \psi_{\mathrm{w}}(x_s)\mathrm{d}s\,\mathrm{d}\rho\right].$$

(9)

### 2.3. Nonhydrodynamic modifications of concentration profile and concentration depletion

The polyelectrolyte length $L$ is held constant at 1 μm, and $L/R_{\mathrm{p}}$ is chosen to be 200 satisfying the condition of thin rod. Our model is applied to the rodlike polyelectrolyte with finite rod diameter, nevertheless, we take here the condition of high aspect ratio. The reason is that the electrostatic potential expressible as a linear superposition of individual potentials of the rod and the wall should be obeyed for the wide range of Debye length. The value of $A_{\mathrm{H}}/kT$ equals to 2.06, based on the Hamaker constant for the case of fused silica interacting through an aqueous medium (i.e. $A_{\mathrm{H}} \cong 8.49 \times 10^{-21}$ J) [17]. For the integration over a whole orientational space, 24-point Gauss–Legendre quadrature was used.

Fig. 2 shows the dimensionless monomer concentration profile along the dimensionless lateral distance $x^*$ with different relative rod lengths $L^*$ normalized by the half width of channel as well as solution ionic strengths. The potentials of $\psi_{\mathrm{s,w}} = 4.0$ and $\psi_{\mathrm{s,p}} = 2.0$ equal to the dimensional values of $4(kT/e)$ and $2(kT/e)$ mV, in respect. The solu-

tion ionic strength ranges from 4.0 μM to 10 mM corresponding to the Debye length $\kappa^{-1}$ range between 152.5 to 3.05 nm for 1–1 type electrolyte. The electrolyte concentration of 4.0 μM in the suspension almost corresponds to the weak screening limit. In the case of extremely repulsive interaction like as $L^* = 0.8$ with ionic strength of 4.0 μM, the concentration does not reach its bulk-solution value even at the center region of the channel. Therefore, this case is needed to include the interaction with a wall located at opposite side.

The concentration depletion becomes more pronounced with the increase of relative rod length, which means the increase of the confinement of slit channel. The overall monomer concentration profile exhibits a shift, and the position where the concentration reaches the bulk concentration moves more closely towards the center region far from the wall as the ionic strength decreases. This behavior results from the increase in electrostatic repulsion as the ionic strength decreases. As the solution ionic strength increases in the limit value (i.e. above 10 mM), the concentration profile is
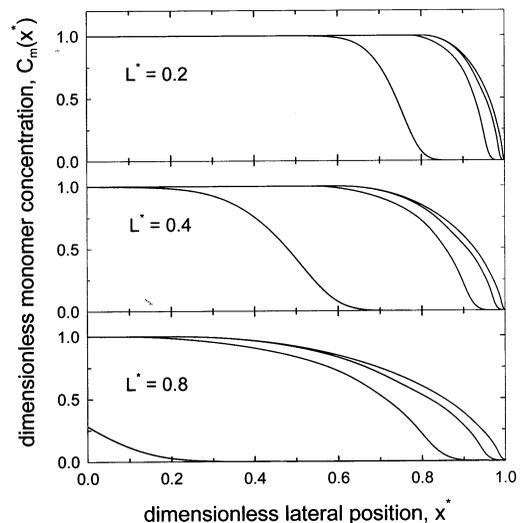


Fig. 2. The monomer density profile for several solution ionic strengths with $L = 1$ μm; half width of channel = 5, 2.5 and 1.25 μm; $\psi_{\mathrm{s,w}} = 4.0$; and $\psi_{\mathrm{s,p}} = 2.0$. The solution ionic strengths are given 4.0 μM, 0.1, 1.0, and 10 mM from left to right curve.
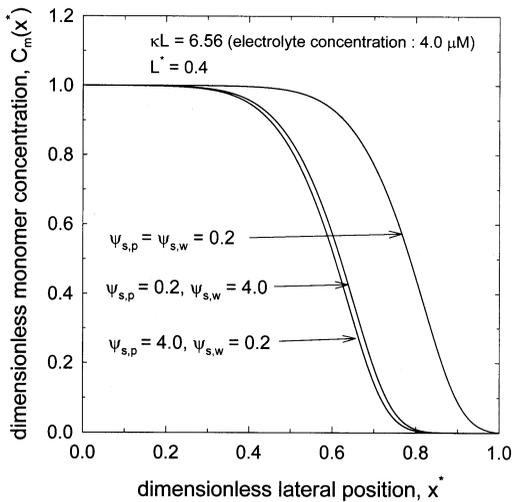
Fig. 3. The monomer density profile for various surface potentials with $L = 1$ μm; half width of channel $= 2.5$ μm; and solution ionic strength of 4.0 μM.

## 3. Orientational order of rodlike polyelectrolyte

In addition to the concentration depletion, the colloidal forces modify the relative orientation of rodlike polyelectrolytes with respect to the confining wall surface. Rodlike polyelectrolytes have uniaxial symmetry around a certain direction denoted by an arbitrary unit vector **n**. As a microscopic viewpoint, the rodlike polyelectrolytes are characterized by the fact that the equilibrium distribution function for the particle direction **u** is not isotropic. The anisotropy is represented by the orientation tensor from which the scalar order parameter $f$ is defined as:

$$f \equiv \frac{3}{2}\left\langle (\boldsymbol{u}\cdot\boldsymbol{n})^2 - \frac{1}{3} \right\rangle. \tag{11}$$

The order parameter is zero for a randomly oriented system, and varies from minus one half for complete transversely isotropic orientation to unity for complete uniaxial orientation. It is convenient to use an orientational order parameter $f$ for uniaxial orientation, defined by:

$$f = \frac{3\langle \cos^2 \theta \rangle - 1}{2}. \tag{12}$$

The averaging process denoted $\langle\rangle$ is to be executed with respect to the concentration-weighted orientation of the entire rod segment $\lambda$ located at position $x$. Thus, it can be evaluated as follows:

similar to that of the uncharged inert case. For this non-interacting case, it is given as [10]:

$$C_{\mathrm{m}}(x) = \begin{cases} \dfrac{x}{L}\left[ 1 - \ln\!\left(\dfrac{x}{L}\right) \right] & 0 \le x' \le L \\ 1 & x' \ge L \end{cases}. \tag{10}$$

Fig. 3 illustrates the concentration profile modified by the variation of surface potential, where the effect of respective surface potentials of both the wall and the rod can be seen.

$$\langle \cos^2 \theta \rangle = \frac{\displaystyle\int_{L/2}^{L} y^2 C(\lambda, x)\,\mathrm{d}\lambda}{\displaystyle\int_{L/2}^{L} C(\lambda, x)\,\mathrm{d}\lambda} = \begin{cases} \dfrac{\displaystyle\int_{L/2}^{L-x} y^2 C^{\mathrm{I}}(\lambda, x)\,\mathrm{d}\lambda + \int_{L-x}^{L} y^2 C^{\mathrm{II}}(\lambda, x)\,\mathrm{d}\lambda}{\displaystyle\int_{L/2}^{L-x} C^{\mathrm{I}}(\lambda, x)\,\mathrm{d}\lambda} & x' < \dfrac{L}{2} \\[4ex] \dfrac{\displaystyle\int_{L/2}^{x} y^2 C^{\mathrm{III}}(\lambda, x)\,\mathrm{d}\lambda + \int_{x}^{L} y^2 C^{\mathrm{II}}(\lambda, x)\,\mathrm{d}\lambda}{\displaystyle\int_{L/2}^{x} C^{\mathrm{III}}(\lambda, x)\,\mathrm{d}\lambda + \int_{x}^{L} C^{\mathrm{II}}(\lambda, x)\,\mathrm{d}\lambda} & \dfrac{L}{2} < x' < L \\[4ex] \dfrac{\displaystyle\int_{L/2}^{L} y^2 C^{\mathrm{III}}(\lambda, x)\,\mathrm{d}\lambda}{\displaystyle\int_{L/2}^{L} C^{\mathrm{III}}(\lambda, x)\,\mathrm{d}\lambda} & x' > L \end{cases} \tag{13}$$

where $y$ denotes $\cos\theta$.

Fig. 4 shows a physical situation of the orientational behavior with the lateral position by presenting at a time both profiles of monomer density and orientational order parameter. When the rod exists near the wall, the repulsive force creates the preferential alignment of rod segments perpendicular to the wall. As the position of rod moves toward to the center region, however, the parallel ordering is favorably occurred. In this case, the minimum value of $f$ corresponds to nearly the same range of the mean depleted layer thickness of concentration profile. If the rod is found enough far from the wall, the random ordering is obviously observed.

Fig. 5 summarizes how the $f$ is changed as a function of lateral distance with variations of relative rod length $L^*$ and solution ionic strength for the same condition of Fig. 2. With the increase of either the strength of confinement or the electrostatic repulsion, the region of perpendicular alignment of the rod is considerably enlarged, which directly reveals the expansion of concentration-depleted layer. As the solution ionic strength decreases, the minimum value of $f$ associated with parallel ordering moves toward center region, resulting from the increase in electrostatic repulsion. Also, the region of parallel ordering gets wider with
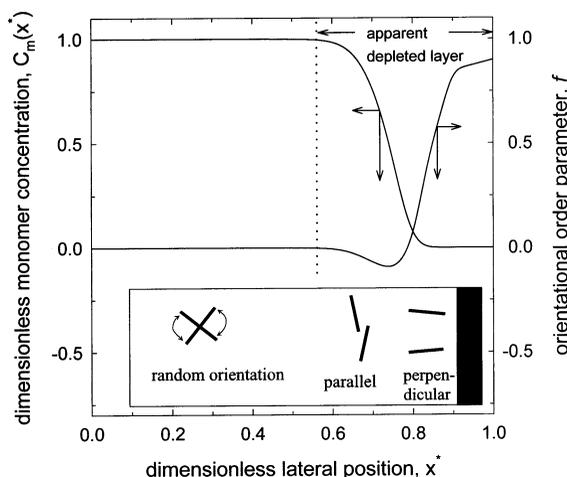


Fig. 4. The monomer density profile and the corresponding orientational order parameter $f$ with $\kappa L = 6.56$, $L = 1$ μm, half width of channel = 5 μm, $\psi_{s,w} = 4.0$, and $\psi_{s,p} = 2.0$. The schematic diagram shows a physical situation of the orientational behavior with the lateral position.
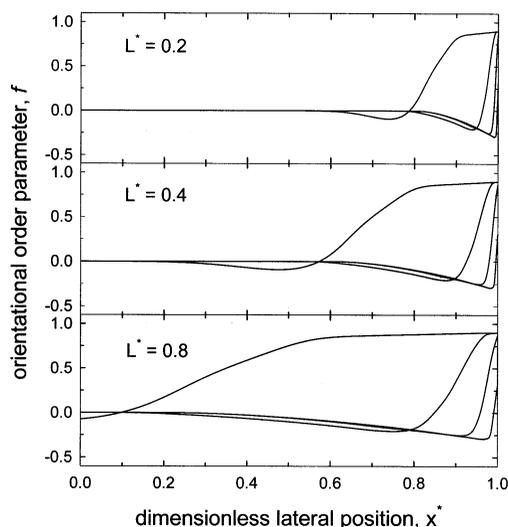


Fig. 5. The profile of orientational order parameter for several solution ionic strengths with $L = 1$ μm, half width of channel = 5, 2.5, and 1.25 μm, $\psi_{s,w} = 4.0$, and $\psi_{s,p} = 2.0$. The solution ionic strengths are given 4.0 μM, 0.1, 1.0, and 10 mM from left to right curve.

the increase of relative rod length. As described above, the solution ionic strength over 10 mM could be almost equivalent to the onset of steric interaction. Once the long-range colloidal interactions do not exist, the $f$ can be obtained from the analytical integration of Eq. (13) with $\Delta\Phi = 0$, that is rewritten as:

$$f = \frac{1}{4}\left[\frac{1 - (x/L)^2 + 2\ln(x/L)}{1 - \ln(x/L)}\right] \tag{14}$$

The result of orientational order explains an agreement with the dimensionless monomer concentration in that the rods can exist close to the wall when the ionic strength is increased. Regarding the change of surface potentials, the perpendicular alignment of rod segments becomes more strengthened as well as broad-ranged as the surface potential increases.

For more description on the behavior of concentration depletion and orientation of rods, the penetration depth $P$ relevant to the degree of accentuation in concentration profile itself needs to be calculated. It can be obtained by integrating over the boundary layer of concentration depletion according to:

$$P = \int_{1-d}^{1} C_m(x^*)dx^*. \tag{15}$$

Here, the apparent depleted layer thickness $d$ is determined as the lateral distance from the wall to the position where the concentration reaches the bulk concentration, which equals to the relative rod length $L^*$ for uncharged non-interacting case. The penetration depth $P$ provides a sensitive measure of small changes in the concentration profile. The penetration depth can not be provided at $L^* = 0.8$ with ionic strength of 4.0 μM because the concentration is depleted almost the whole inside a channel as shown in Fig. 2. Fig. 6 reveals that the penetration depth is entirely increased as the strength of confinement increases. Upon the changing of electrostatic repulsion, the penetration depth is constant for solution ionic strength over 0.1 mM, while it tends to be increased for lower ionic strength less than 0.1 mM. Comparing with Fig. 5, it turns out that the alteration of penetration depth is closely related to the orientation of rods. The increase of orientation perpendicular to the wall yields the increasing of penetration depth.

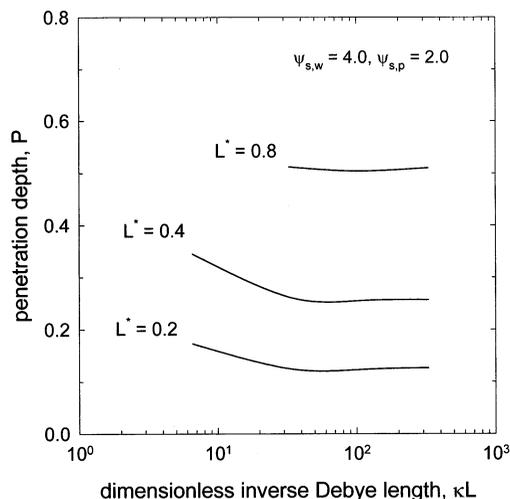Since probes of novel experimental apparatus such as X-ray reflectance and FTIR-ATR are sensitive to segmental anisotropy near the solid surface, the observation on the orientation of dilute polyelectrolytes seems possible. Not that combining the experimental observation on the orientation and the concentration depletion will provide the guaranteed verification on theoretical predictions.

## 4. Partition coefficients of rodlike polyelectrolyte

The partition coefficient of rodlike polyelectrolytes provides an important information relevant to hindered diffusion, size analysis in size-exclusion chromatography, and colloids characterization by means of membrane filtration. The partition coefficient $K$, defined as the ratio of mean concentration between the confined channel and the bulk at equilibrium, can be expressed as:

$$K \equiv \frac{\iint \exp(-\Phi/kT)d\boldsymbol{x}d\boldsymbol{\xi}}{\iint d\boldsymbol{x}d\boldsymbol{\xi}} \tag{16}$$

where $\boldsymbol{x}$ and $\boldsymbol{\xi}$ mean coordinate vectors describing particle position and orientation, respectively. The partitioning of charged, finite concentrated solutes with spherical shape in slit or cylindrical pores has been investigated in the previous studies [13,14], where it is found that the electrostatic interactions play a major ingredient in cases of aqueous colloidal suspensions.

The concentration depletion near a wall does determine the concentration partitioning, as a consequence, the partition coefficient for rodlike polyelectrolytes in the slit channel is expressed as:

$$K = \frac{\int_0^1 C_m(x^*)dx^*}{\int_0^1 dx^*}. \tag{17}$$

When a steric interaction purely determines the partitioning in the dilute limit, Eq. (17) readily reduces to $K = 1 - (1/2)(L/\text{channel width})$ if the channel width is larger than $2L$.

Fig. 7 illustrates the partition coefficients as a function of the ratio of rod length to channel width ranging up to 0.5 with different dimensionless inverse Debye lengths (or, solution ionic
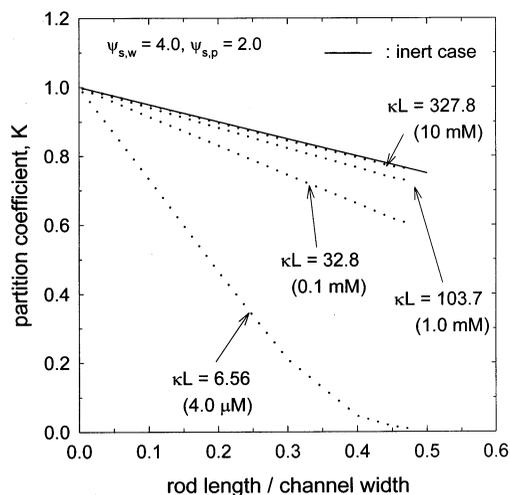


Fig. 6. The penetration depth P as a function of dimensionless inverse Debye lengths with $L^* = 0.2$, 0.4, and 0.8. The conditions are same to the case of Fig. 2.

Fig. 7. The partition coefficient $K$ at various dimensionless inverse Debye lengths as a function of the ratio of rod length to channel width.

strengths), where the rod length $L$ is constant at 1 μm. It can be seen that, firstly, the rod is more excluded by electrostatic and entropic effects with the increase of rod length. Strong repulsion between the rod and the wall leads to a dramatic decrease in the partitioning for lower ionic strength of 4.0 μM. The rod-wall interaction becomes repulsive for low ionic strength, consequently the rod will exist near the center region of the channel. Then, the partition coefficient decreases since the rod can hardly be inserted into the channel. On the contrary, the rod can be found near the wall for high ionic strength, and the partition coefficient increases accordingly. As $\kappa L$ increases furthermore, the partition coefficient approaches to the inert non-interacting result, as one could expect. Fig. 7 suggests that we need to be careful on the electrostatic effect even at moderate ionic strength, when charged complex fluids are partitioned in confined spaces. In addition, the partition coefficient will also be changed with variation of surface potentials of both the wall and the rod, although not given here. At a given $\kappa L$, the partition coefficient will decrease with the increase of surface potentials. Although appropriate data enabling a rigorous verification of Fig. 7 are not addressed, the problem of polyelectrolyte

partitioning can be a subject of both theoretical and experimental studies.

## 5. Conclusions

In order to investigate the microstructural behavior of rodlike polyelectrolyte in confined spaces, both the orientational order and the partitioning have been examined by extending the previous study on the monomer concentration profile. Our theoretical predictions show that the effect of long-range physicochemical interactions between the wall and the polyelectrolyte plays an important role in the concentration depletion. The monomer concentration profiles shift toward the center of the slit microchannel so that the depleted layer thickness increases either with decreased solution ionic strength or with increased surface potentials of a wall and the rod.

The analysis on the rod orientation allows us to understand the change of monomer concentration profile. For purely steric case, the parallel alignment is favored near the wall due to the entropic surface exclusion. The electrostatic repulsive forces create the preferential alignment of rod segments perpendicular to the plane of wall, which results in the enlargement of concentration-depleted layer. The orientation behavior can be explained by the alternation of penetration depth, which is relevant to the degree of accentuation in concentration profile itself. From the monomer concentration profile within a slit microchannel, the concentration partitioning between the bulk and the confined channel can be evaluated. It has been seen that the presence of electrostatic interactions significantly affects the partitioning behavior. With the increase of either the strength of confinement or the electrostatic repulsion, there is little probability that the rod can exist within the channel, and consequently the partition coefficient is decreased.

## Acknowledgements

## References

[1] R.G. Larson, The Structure and Rheology of Complex Fluids, Oxford University Press, New York, 1999.

[2] L. Auvray, J. Phys. (Paris) 42 (1981) 79.

[3] J.C. Giddings, E. Kucera, C.P. Russell, M.N. Myers, J. Phys. Chem. 72 (1968) 4397.

[4] E.F. Casassa, J. Polym. Sci., Part A-2 10 (1972) 381.

[5] F. Rondelez, D. Ausserré, H. Hervet, Ann. Rev. Phys. Chem. 38 (1987) 317.

[6] D. Ausserré, J. Edwards, J. Lecourtier, H. Hervet, F. Rondelez, Europhys. Lett. 14 (1991) 33.

[7] K.S. Sorbie, J. Coll. Interf. Sci. 139 (1990) 299.

[8] J.J. de Pablo, H.C. Öttinger, Y. Rabin, AIChE J. 38 (1992) 273.

[9] M.-S. Chun, O.O. Park, S.-M. Yang, J. Coll. Interf. Sci. 161 (1993) 247.

[10] D.A. Hoagland, Macromolecules 23 (1990) 2781.

[11] J.L. Anderson, J.H. Brannon, J. Polym. Sci., Polym. Phys. Eds. 19 (1981) 405.

[12] F.G. Smith, W.M. Deen, J. Coll. Interf. Sci. 91 (1983) 571.

[13] M.-S. Chun, R.J. Phillips, AIChE J. 43 (1997) 1194.

[14] M.-S. Chun, Macromol. Theory Simulations 8 (1999) 418.

[15] K.W. Limbach, J.M. Nitsche, J. Wei, AIChE J. 35 (1989) 42.

[16] W.B. Russel, D.A. Saville, W.R. Schowalter, Colloidal Dispersions, Cambridge University Press, London, 1989.

[17] R.J. Hunter, Foundations of Colloid Science, vols. 1–2, Clarendon Press, Oxford, 1989.